Single-Component Organic Semiconductors Based on Novel Radicals that Exhibit Electrochemical Amphotericity: Preparation, Crystal Structures, and Solid-State Properties of *N,N′*-Dicyanopyrazinonaphthoquinodiiminides Substituted with an *N*-Alkylpyridinium Unit

Takanori Suzuki*

Division of Chemistry, Graduate School of Science, Hokkaido University,Sapporo 060-0810, Japan

Setsuko Miyanari, Yoshiaki Tsubata, Takanori Fukushima, and Tsutomu Miyashi

Department of Chemistry, Graduate School of Science, Tohoku University, Aoba-ku, Sendai 980-8578, Japan

Yoshiro Yamashita

Department of Chemistry, Interdisciplinary Graduate School of Science and Engineering, Tokyo Institute of Technology, Midori-ku, Yokohama 226-8502, Japan

Kenichi Imaeda

Institute for Molecular Science, Myodaiji, Okazaki 444-8585, Japan

Takayuki Ishida and Takashi Nogami

Department of Applied Physics and Chemistry, The University of Electro-Communications, Chofugaoka, Chofu 182-8585, Japan

tak@sci.hokudai.ac.jp.

Received September 12, 2000

N,N′-Dicyanonaphthoquinodiimines fused with a pyrazine ring **1** were prepared from the corresponding quinones **4**. The new acceptors **1** have a planar π-system and undergo reversible two-stage 1e-reduction. Quaternization of the pyridyl substituent in **1d**−**f** gave pyridinium derivatives **2d**$^+$, **2e**$^+$, and R-**3**$^+$, respectively, which are stronger acceptors that undergo three-stage 1e-reduction. Upon electrochemical reduction of these cations, novel radicals **2d**$^\bullet$, **2e**$^\bullet$, and R-**3**$^\bullet$ were generated and isolated as stable solids. The molecular geometries determined by X-ray analysis indicated that these radicals adopt a zwitterionic structure, in which the unpaired electron is located on the quinodiimine unit but not on the pyridyl group. These novel radicals undergo facile and reversible 1e-oxidation as well as two-stage 1e-reduction. The observed amphotericity endows the radicals with electrical conductivities (10^{-5} to 10^{-9} S cm^{-1}), and these thus represent a new motif for single-component organic semiconductors.

Recently, much attention has been focused on multistage organic redox systems in the field of materials science. Among these, a series of compounds that show electrochemical amphotericity is of special interest,[1] where 1e-oxidation and reduction occur within an easily accessible potential window. Beside their potential application as NLO materials[2] or molecular electronic devices,[3] another unique property is their electrical conductivity[4] as a single component.[5−8] Although it is quite difficult to endow closed-shell species with high amphotericity,[1] this would be much easier to achieve with stable radicals. Furthermore, intrinsic conductivity is warranted in such open-shell species because the unpaired electron could become a carrier in the solid.[7,8] From this viewpoint, we previously studied a series of (A-π-D$^\bullet$)-type stable radicals **5** which have a pyrazino-TCNQ skeleton (Scheme 1). Form A can polarize to a zwitterionic structure, form B, by configuration interac-

(1) Nakasuji, K.; Yoshida, K.; Murata, I. *J. Am. Chem. Soc.* **1983**, *105*, 5136. Takahashi, K.; Suzuki, T. *J. Am. Chem. Soc.* **1989**, *111*, 5483. Bando, P.; Martín, N.; Segura, J. L.; Seoane, C.; Ortí, E.; Viruela, P. M.; Viruuela, R.; Albert, A.; Cano, F. H. *J. Org. Chem.* **1994**, *59*, 4618. Karikome, K.; Kitamura, C.; Tanaka, S.; Yamashita, Y. *J. Am. Chem. Soc.* **1995**, *117*, 6791.

(2) Marder, S. R.; Kippelen, B.; Jen, A. K.-Y.; Peyghambarian, N. *Nature* **1997**, *388*, 845.

(3) Petty, M. C.; Bryce, M. R.; Bloor, D. *Introduction to Molecular Electronics*; Oxford University Press: Oxford, 1995.

(4) Farges, J. P. *Organic Conductors: Fundamental and Applications*; Marcel Dekker: New York, 1994.

(5) Inokuchi, H.; Imaeda, K.; Enoki, T.; Mori, T.; Maruyama, Y.; Saito, G.; Okada, N.; Yamochi, H.; Seki, K.; Higuchi, Y.; Yasuoka, N. *Nature* **1987**, *329*, 39. Yamashita, Y.; Tanaka, S.; Imaeda, K.; Inokuchi, H. *Chem. Lett.* **1991**, 1213. Cordes, A. W.; Haddon, R. C.; Oakley, R. T.; Schneemeyer, L. F.; Waszczak, J. V.; Young, K. M.; Zimmerman, N. M. *J. Am. Chem. Soc.* **1991**, *113*, 582.

(6) Morimoto, K.; Inabe, T. *J. Mater. Chem.* **1995**, *5*, 1749. Kobayashi, A.; Tanaka, H.; Kumasaki, M.; Torii, H.; Narymbetov, B.; Adachi, T. *J. Am. Chem. Soc.* **1999**, *121*, 10763.

(7) Awaga, K.; Sugano, T.; Kinoshita, M. *Bull. Chem. Soc. Jpn.* **1985**, *58*, 1886.

(8) Tsubata, Y.; Suzuki, T.; Miyashi, T.; Yamashita, Y. *J. Org. Chem.* **1992**, *57*, 6749.

10.1021/jo001352r CCC: $20.00
Published on Web 12/16/2000

Scheme 1

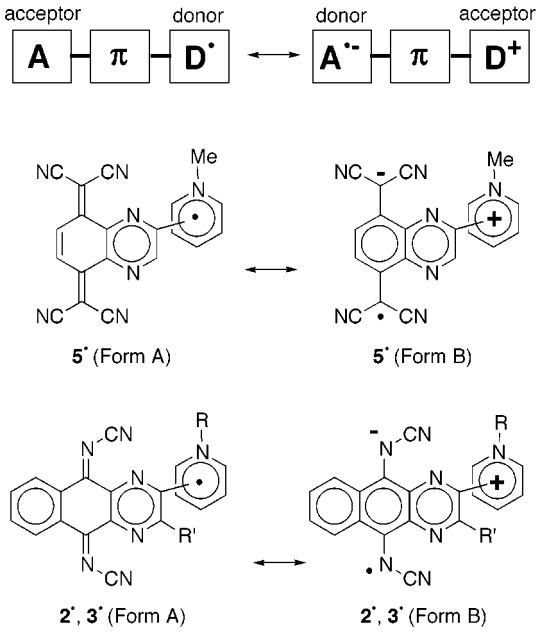

tion. In both forms, electron-donating and -accepting subunits are present to ensure electrochemical amphotericity, which forms the core of our molecular design. Radicals **5** were proven to be conductive as expected (10^{-5} to 10^{-9} S cm^{-1}),[8] yet the difficulty of obtaining single crystalline samples hampered the detailed measurement of their solid-state properties as well as the determination of their precise molecular geometries. In our continuing efforts to generate and characterize novel stable radicals with high electrical amphotericity,[9] we have found that *N*,*N*′-dicyanonaphthoquinodiimine (DCNNQI) fused with a pyrazine ring is a special skeleton that gives highly crystalline radicals of (A-π-D•) ↔ ($A^{-\bullet}$-π-D^{+})-type (Scheme 1). We report here the preparation, properties, and molecular and crystal structures of the title radicals **2**• and **3**•, which are new members of a rare class of semiconductors based on single-component pure organic materials.

Results and Discussion

Preparation, Structure, and Redox Behavior of Pyrazino-DCNNQIs (1). New DCNNQI derivatives fused with a pyrazine ring **1** were prepared by Hünig's method[10] from the corresponding pyrazinonaphthoquinones **4** and bis(trimethylsilyl)carbodiimide **6** under the influence of $TiCl_4$ or CsF. Probably due to the strong coordination of Ti to N atoms of pyrazine and/or pyridine rings, however, the reaction conditions had to be examined and adjusted for this series of quinones **4a**−**f**. Thus, the diphenyl derivative **1b** was obtained in 72% yield when quinone **4b**[11] was first complexed with $TiCl_4$ in CH_2Cl_2 and then heated with **6**. However, treatment of the parent quinone **4a**[11] by a similar procedure gave an intractable black tar. THF was shown to be a better

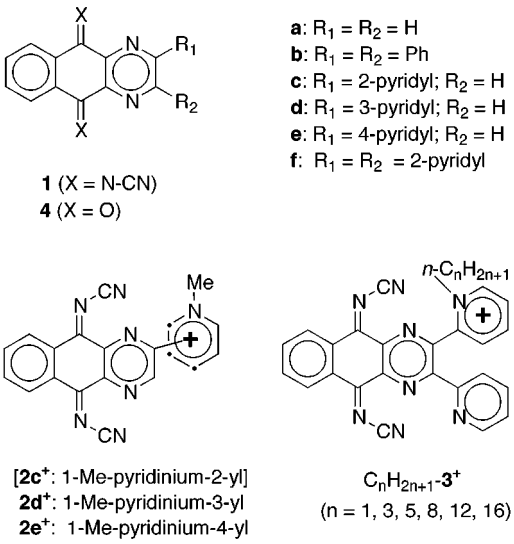

reaction medium in this case, and precomplexation of $TiCl_4$ with THF, but not with quinone, is effective for obtaining the unsubstituted pyrazino-DCNNQI **1a** in an acceptable yield (40%). The latter conditions also worked well for preparing compounds **1c**−**e** with a pyridil substituent from the corresponding quinones **4c**−**e**, which in turn were obtained by condensation reactions of 2,3-diaminonaphthoquinone[12] and bromoacetylpyridines in DMSO. Treatment of the diamine with 2,2′-pyridil gave quinone **4f** with two pyridine rings, which was converted to DCNNQI derivative **1f** by carbodiimide **6** in the presence of CsF but not $TiCl_4$. The DCNNQIs **1** thus prepared are stable orange crystals, but are sensitive to acid-catalyzed hydrolysis. They were best purified by recrystallization, since chromatographic separation caused partial decomposition of **1**.

A planar geometry is expected for the pyrazino-DCNNQI skeleton by considering the reported planarity for the parent DCNNQI[13] and pyrazino-TCNQ[8] skeletons. This idea was confirmed by an X-ray analysis of **1f**: the largest deviation of an atom from the least-squares plane is only 0.03 Å for the pyrazino-DCNNQI unit (Figure S1 in the Supporting Information). Due to the *o*-terphenyl-type structure, each of two pyridyl groups makes a dihedral angle of 49.3° or 30.6° with the pyrazine ring (Scheme 2). For comparison, an X-ray analysis was also conducted for **7f** with a tetracyanonaphthoquinodimethane (TCNNQ) skeleton (Figure S2), which was readily prepared by the condensation reaction of quinone **4f** with malononitrile. As shown in Scheme 2, the central six-membered ring of pyrazino-TCNNQ **7f** exhibits boat-form deformation, which is caused by steric repulsion between the *peri*-hydrogens and dicyanomethylene groups.[14,15] Two pyridyl groups are rotated against the pyrazine ring by 54.5° and 26.5° in **7f**, which are similar to the values observed in **1f**.

In accord with the planar π-system for the pyrazino-DCNNQI skeleton, **1a** undergoes reversible two-stage 1e-

(9) Amphoteric radicals exhibiting inverse polarization [(D-π−$A^{\bullet}$) ↔ ($D^{+\bullet}$-π−A^{-}); D = TTFs] were generated and characterized: Suzuki, T.; Yamada, M.; Ohkita, M.; Tsuji, T. *Heterocycles* **2001**, *54*, 387.

(10) Aumüller, A.; Hünig, S. *Angew. Chem., Int. Ed. Engl.* **1984**, *23*, 447; *Liebigs Ann. Chem.* **1986**, 142.

(11) Efimova, G. A.; Efros, L. S. *Zh. Org. Khim.* **1966**, *2*, 531 [*CA* **65**: 8910a].

(12) Winkelmann, E. *Tetrahedron* **1969**, *25*, 2427.

(13) Aumüller, A.; Hünig, S. *Angew. Chem., Int. Ed. Engl.* **1984**, *23*, 449.

(14) Schubert, U.; Hünig, S.; Aumüller, A. *Liebigs Ann. Chem.* **1985**, 1216.

(15) Iwasaki, F. *Acta Crystallogr.* **1971**, *B27*, 1360. Kabuto, C.; Fukazawa, Y.; Suzuki, T.; Yamashita, Y.; Miyashi, T.; Mukai, T. *Tetrahedron Lett.* **1986**, *27*, 925.

Table 1. Reduction Potentials[a] of Newly Prepared DCNNQIs 1a,b,f and Related Acceptors Measured in MeCN

compound	E_1^{red}/V	E_2^{red}/V
1a ($R_1 = R_2 = H$)	−0.14	−0.61
1b ($R_1 = R_2 = Ph$)	−0.15	−0.62
1f ($R_1 = R_2 = 2$-pyridyl)	−0.11	−0.59
7a	−0.25	−0.32
DCNQI	+0.18	−0.47
DCNNQI	+0.02	−0.56

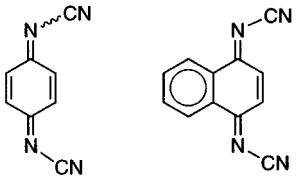

[a] E/V vs SCE, 0.1 mol dm^{-3} Et_4NClO_4 in MeCN, Pt electrode, scan rate 100 mV s^{-1}.

Scheme 2

Dihedral angles (°) in **1f** and **7f**

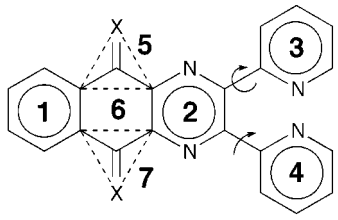

X =	N-CN	$C(CN)_2$
plane 1 and 2	13.3	23.6
plane 2 and 3	49.3	54.5
plane 2 and 4	30.6	26.5
plane 5 and 6	2.3	22.9
plane 6 and 7	3.4	21.4

reduction (Table 1). Essentially the same first and second reduction potentials (E_1^{red} and E_2^{red}) were observed for the diphenyl and bis(2-pyridyl) derivatives **1b** and **1f**, which shows that the bulky substituents on the pyrazine ring no longer affect the intrinsic redox properties of pyrazino-DCNNQI. As indicated by comparison of E_1^{red} values measured under the same conditions, **1** are weaker acceptors than DCNQI[10] and DCNNQI,[10] which obeys the general trend that annelation of an aromatic ring raises the LUMO level of Wurster-type acceptors.[16,17] In the case of pyrazino-TCNNQ **7a**, which has a deformed structure, the difference between E_1^{red} and E_2^{red} (ΔE) is so small that its anion radical easily undergoes disproportionation.[18,19] On the contrary, the large ΔE values of **1** indicate that their anion radicals are thermodynamically stable. In fact, **1b**$^{-\bullet}$ was isolated as a stable green-black salt [Et_4N^+(**1b**)$_2^{-\bullet}$: λ_{max} (DMF) 588 (log ϵ 4.32), 534 (4.14), 450 sh (4.01) nm] when **1b** was electrochemically reduced in CH_2Cl_2 containing 0.05 mol dm^{-3} Et_4NClO_4.

The observed planar geometry as well as stable anion radical formation support the use of a pyrazino-DCNNQI skeleton in constructing (A-π-D$^{\bullet}$) ↔ (A$^{-\bullet}$-π-D$^+$)-type stable radicals.

Preparation, Redox Properties, and Molecular Structure of Stable Radicals (2$^{\bullet}$ and 3$^{\bullet}$). Treatment of pyrazino-DCNNQIs possessing a 3-pyridyl or 4-pyridyl substituent (**1d** and **1e**) with CH_3OTf in CH_2Cl_2 gave quaternary salts, **2d**$^+$ and **2e**$^+$, as yellow powders in respective yields of 71 and 91%. Alkylation occurs selectively at the pyridine N atom, as shown by their NMR spectra. In the case of **1c** with a 2-pyridyl substituent, however, *N*-methylation did not proceed cleanly even under other conditions using Me_3OBF_4 or Me_2SO_4 as an alkylating reagent. Therefore, we could not obtain a pure salt of **2c**$^+$ although bis(2-pyridyl) derivative **1f** was easily converted to the monomethylated cation CH_3-**3**$^+$ in 82% yield.

Table 2. Redox Potentials[a] of Acceptors 1c−f, *N*-methylated Cations (2d$^+$, 2e$^+$, CH_3-3$^+$), and Radicals (2d$^{\bullet}$, 2e$^{\bullet}$, CH_3-3$^{\bullet}$) Measured in DMF along with the Electrical Conductivities[b] of Radicals

compound	E_1^{ox}/V	E_1^{red}/V	E_2^{red}/V	E_3^{red}/V	σ/S cm^{-1}
1c	−	+0.02	−0.51	−	−
1d	−	+0.01	−0.53	−	−
2d$^+$	−	+0.10	−0.41	−1.22[c]	−
2d$^{\bullet}$	+0.10	−0.39	−1.20[c]	−	5.9×10^{-6}
1e	−	+0.03	−0.50	−	−
2e$^+$	−	+0.12	−0.36	−1.01[c]	−
2e$^{\bullet}$	+0.12	−0.36	−1.01[c]	−	1.6×10^{-5}
1f	−	−0.06	−0.59	−	−
CH_3-**3**$^+$	−	+0.09	−0.45	−1.33[c]	−
CH_3-**3**$^{\bullet}$	+0.09	−0.44	−1.35[c]	−	6.5×10^{-6}

[a] E/V vs SCE, 0.1 mol dm^{-3} Et_4NClO_4 in DMF, Pt electrode, scan rate 100 mV s^{-1}. [b] Measured on compaction pellets by a two-probe method at room temperature. [c] Irreversible or quasi-reversible waves. Values are calculated as $E^{red} = E^{pc}$(cathodic peak potential) + 0.03 V.

According to voltammetric analyses on pyridinium derivatives (**2d**$^+$, **2e**$^+$, CH_3-**3**$^+$), they undergo three-stage 1e-reduction (Table 2). The slightly higher values of E_1^{red} and E_2^{red} compared with those for **1d**−**f** are due to the strong electron-withdrawing nature of the *N*-methylpyridinium substituent. The third reduction potentials (E_3^{red}) of these cations are close to E^{red} of *N*-methylpyridinium iodide (−1.27 V) measured under the same conditions. These results suggest that E_1^{red} and E_2^{red} of cations correspond to two-stage 1e-reduction of the pyrazino-DCNNQI unit, whereas the *N*-methylpyridinium moiety is reduced at E_3^{red} (Scheme 3). The positive shifts of E_2^{red} and E_3^{red} of **2e**$^+$ compared with those of **2d**$^+$ may be accounted for by smaller Coulombic repulsion in **2e**$^-$ due to the contribution of charge-annihilated form C. Considering these points, the main contributor to these radicals seems to be the zwitterionic structure, form B, in which the unpaired electron is located on the pyrazino-DCNNQI skeleton.

Electrochemical reduction of the quaternary salts (**2d**$^+$TfO$^-$, **2e**$^+$TfO$^-$, and CH_3-**3**$^+$TfO$^-$) in MeCN gave black-violet crystalline materials with a low solubility, which were assigned to the desired radicals (**2d**$^{\bullet}$, **2e**$^{\bullet}$, and CH_3-**3**$^{\bullet}$). Their cyclic voltammograms indicated that they undergo facile and reversible 1e-oxidation as well as two-stage 1e-reduction (Figure 1), demonstrating their electrochemical amphotericity. As shown in Table 2, the oxidation potentials (E_1^{ox}) of radicals correspond well to

(16) Deuchert, K.; Hünig, S. *Angew. Chem Int. Ed. Engl.* **1978** *17*, 875.
(17) Aumüller, A.; Hünig, S. *Liebigs Ann. Chem.* **1986**, 165.
(18) Yamashita, Y.; Suzuki, T.; Saito, G.; Mukai, T. *Chem. Lett.* **1986**, 715.
(19) Aumüller, A.; Hünig, S. *Liebigs Ann. Chem.* **1984**, 618.

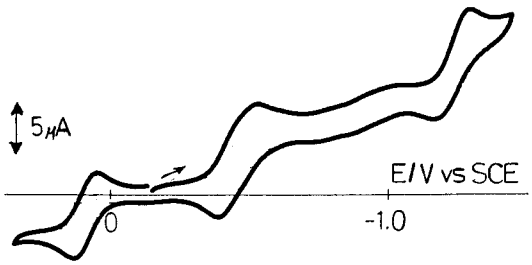

Figure 1. Cyclic voltammogram of **1d**• first scanned to negative (E/V vs SCE, 0.1 mol dm^{-3} Et_4NClO_4 in DMF, Pt electrode, scan rate 100 mV s^{-1}).

Scheme 3

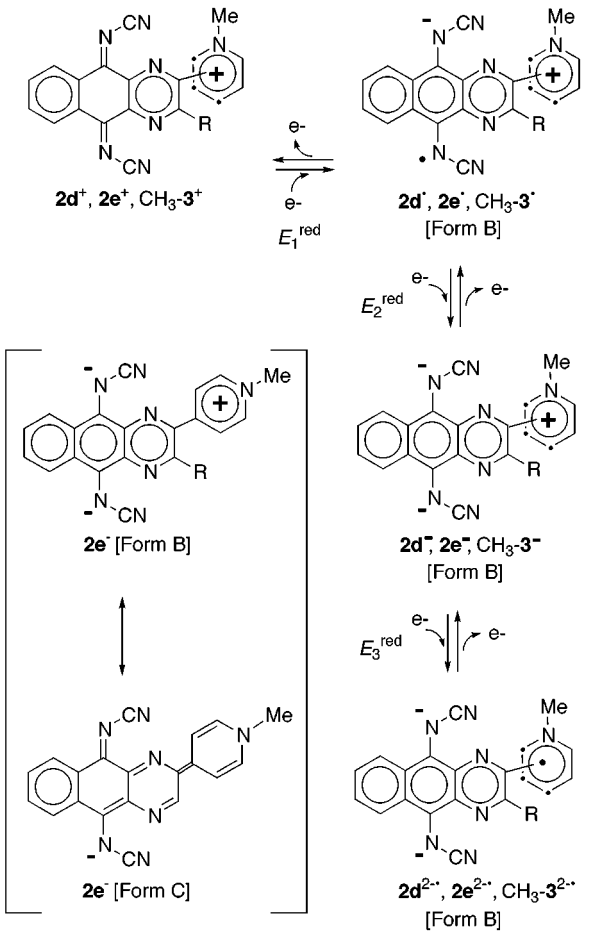

E_1^{red} of cations as expected, and E_1^{red} and E_2^{red} of radicals are nearly the same as E_2^{red} and E_3^{red} of cations, respectively. On the basis of the redox properties of **2d**•, **2e**•, and CH_3-**3**•, it was confirmed that these species exist as monomers rather than as covalently bound dimers.

The contribution of form B to the novel radical was indicated by the resemblance of the UV−vis spectra to that of **1b**$^{-\bullet}$ [CH_3-**3**•: λ_{max} (DMF) 596 (log ϵ 4.09), 550 (3.94), 460 (3.76) nm]. Such strong absorptions in the longer wavelength region are absent in cationic precursors or neutral DCNNQIs (Figure 2). An X-ray analysis of CH_3-**3**• confirmed that the radical adopts a zwitterionic structure, form B (Figure S3). Notably, the exocyclic imine bonds [av. 1.331(10) Å] are longer than those in **1f** [av. 1.297(3) Å]. The latter value is close to that found in the parent DCNQI [1.303(2) Å][20] whereas those found in CH_3-**3**• are comparable to that in the anion radical salt [Li^+(2,5-Me_2-DCNQI)$^{-\bullet}$: 1.323(3) Å].[21] Since this bond

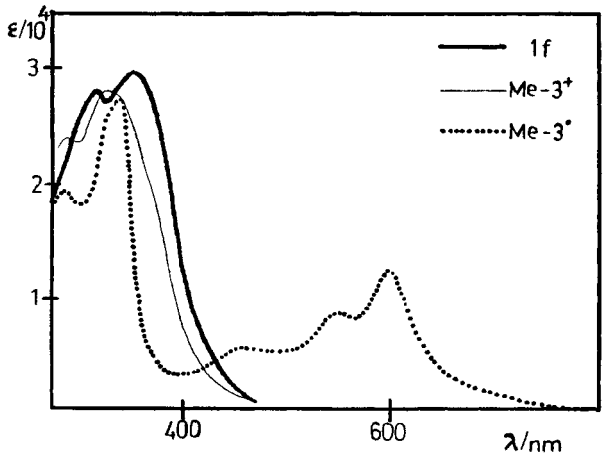

Figure 2. UV−vis spectra of **1f**, CH_3-**3**$^+$OTf$^-$, and CH_3-**3**• measured in DMF.

Scheme 4

Structural parameters in R-**3**•

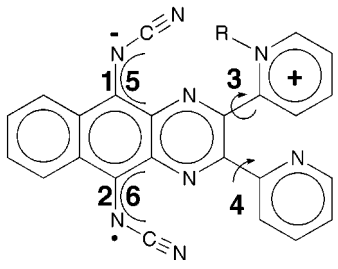

R =	CH_3	C_5H_{11}
bond length 1 / Å	1.329(10)	1.322(8)
bond length 2 / Å	1.332(9)	1.332(8)
dihedral angle 3 / °	78.8	69.7
dihedral angle 4 / °	30.3	27.6
torsion angle 5/ °	18.8	16.4
torsion angle 6/ °	7.4	7.2

length is sensitive to the degree of charge-transfer,[21] it is reasonable to assume that the DCNNQI unit in CH_3-**3**• is completely reduced to its anion radical despite the large experimental errors of the bond lengths. One of the N−C≡N units is slightly deviated from the planar naphtho[2,3-*b*]pyrazine unit, which is also in accord with the single-bond character of the exocyclic imine bonds and the reduced rotation barrier around them. On the other hand, the positive charge seems to localize on the *N*-methylpyridinium moiety, which is attached to the pyrazine ring with a larger dihedral angle (78.8°) than that of the neutral pyridyl group (30.3°) (Scheme 4).

Solid-State Properties and Crystal Structure of Stable Radicals (2• **and 3**•**).** The novel radicals studied here represent new single-component organic semiconductors (Table 2). Although the observed conductivities (ca. 10^{-5} S cm^{-1}) are lower than those of conventional multicomponent organic conductors or single-component solids of transition metal complexes,[6] they are among the highest values ever reported for pure organic materials.[5]

(20) Andreetti, G. D.; Bradamante, S.; Bizzarri, P. C.; Pagai, G. A. *Mol. Cryst. Liq. Cryst.* **1985**, *120*, 309.
(21) Kato, R.; Kobayashi, H.; Kobayashi, A. *J. Am. Chem. Soc.* **1989**, *111*, 5224.

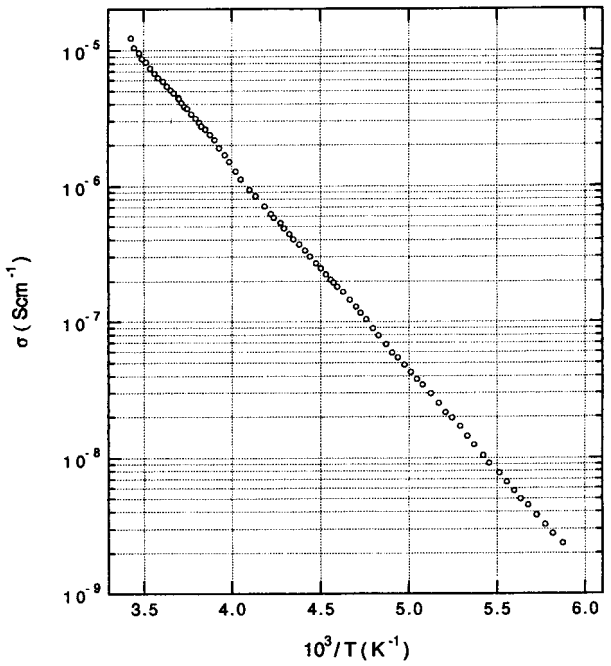

Figure 3. Temperature-dependence of conductivity for single crystalline CH_3-**3**• measured along the needle axis.

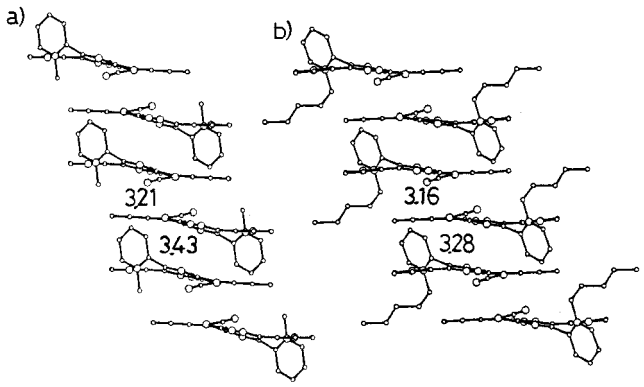

Figure 4. One-dimensional columnar stack in (a) CH_3-**3**• and (b) C_5H_{11}-**3**• crystals.

The temperature-dependence of the single-crystalline sample of CH_3-**3**• revealed that it is a semiconductor with a small activation energy of 0.30 eV, and a linear correlation was seen between the logarithm of the conductivity and $1/T$, as shown in Figure 3. Its room-temperature conductivity (1.2×10^{-5} S cm^{-1}) is only 1.8 times as large as the value obtained with the powder sample, suggesting a low anisotropy of conduction.

In the crystal of CH_3-**3**•, molecules are packed in a one-dimensional columnar stack (Figure 4a), which seems to be the main conduction path by face-to-face overlap of π-electrons. One of the two overlaps in the column is of "ring-over-double bond"-type[22] with a small interplanar distance of 3.21 Å (Figure 5a) and is thus suitable for orbital interaction between DCNNQI$^{-\bullet}$ moieties. In the other overlap (Figure 5b), however, molecules are greatly slipped with a wider separation of molecular planes (3.43 Å). Such dyad formation in the column may be one of the reasons for the limited conductivity of this radical. It should be noted that there are several short contacts

(22) Fritchie, C. J., Jr. *Acta Crystallogr.* **1966**, *20*, 892.

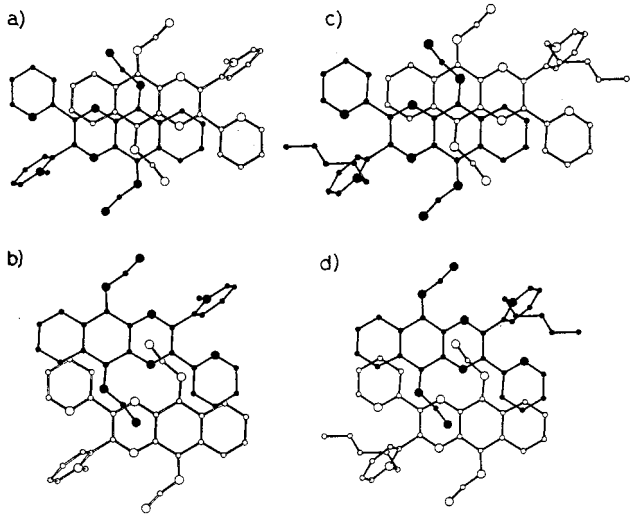

Figure 5. Two types of molecular overlaps in CH_3-**3**• [(a) in the dyad (interplanar distance, 3.21 Å); (b) between the dyads (3.43 Å)] and in C_5H_{11}-**3**• [(c) in the dyad (interplanar distance, 3.16 Å); (d) between the dyads (3.28 Å)]. Molecular planes are arranged parallel in all overlaps.

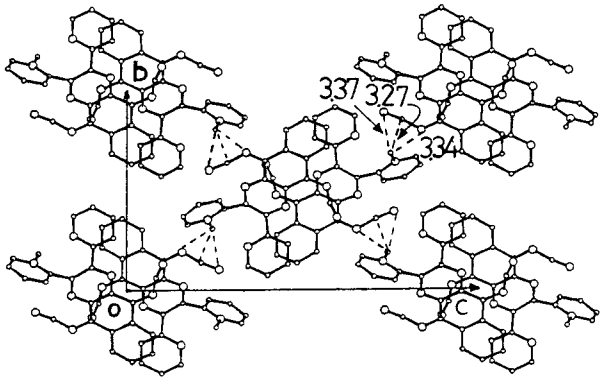

Figure 6. Packing arrangement in CH_3-**3**• crystal viewed along the *a* axis. Intermolecular Me···N (3.34, 3.37 Å) and Me•••C(sp) (3.27 Å) contacts are shown by dotted lines (sum of van der Waals radii: 3.50 Å for Me···N; 3.70 Å for Me···C).

(3.27, 3.34, 3.37 Å) between the N−C≡N moiety and Me group of neighboring columns (Figure 6). By considering the high acidity of C−H in Me of pyridinium, it is likely that such contacts induce C−H···N-type hydrogen bonding.[23] Thus, the suggested small anisotropy of conduction in CH_3-**3**• may be related to the proximity of columnar stacks in the crystal, which may induce conductivity in the transverse direction.

To confirm this idea, radicals C_nH_{2n+1}-**3**• which have a longer alkyl group on the pyridinium moiety were prepared, and their properties were investigated. By quaternization of **1f** with *n*-C_nH_{2n+1}OTf (n = 3, 5, 8, 12, and 16), the corresponding cations C_nH_{2n+1}-**3**$^+$ were obtained as stable yellow triflate salts in respective yields of 40−82% and were in turn converted to the desired radicals C_nH_{2n+1}-**3**• in yields of 46−87% by electrolyses in MeCN. The length of the alkyl group scarcely affects the redox properties of C_nH_{2n+1}-**3**$^+$ and C_nH_{2n+1}-**3**• in solution (Table 3). However, the electrical conductivities of powder samples of these radicals change over several

(23) Muscal, M. *Chem. Commun.* **1998**, 303. Steiner, T.; Desiraju, G. R. *Chem. Commun.* **1998**, 891. Calhorda, M. J. *Chem. Commun.* **2000**, 801.

Table 3. Redox Potentials[a] of Cationic Precursors C_nH_{2n+1}-3$^+$ and Radicals C_nH_{2n+1}-3$^\bullet$ Measured in DMF along with the Electrical Conductivities[b] of Radicals C_nH_{2n+1}-3$^\bullet$

compound	E_1^{ox}/V	E_1^{red}/V	E_2^{red}/V	E_3^{red}/V	σ/S cm^{-1}
C_3H_7-**3**$^+$	−	+0.09	−0.42	−1.34[c]	
C_3H_7-**3**$^\bullet$	+0.09	−0.43	−1.36[c]	−	1.8×10^{-6}
C_5H_{11}-**3**$^+$	−	+0.13	−0.41	−1.28[c]	
C_5H_{11}-**3**$^\bullet$	+0.14	−0.38	−1.26[c]	−	6.0×10^{-8}
C_8H_{17}-**3**$^+$		+0.09	−0.45	−1.32[c]	
C_8H_{17}-**3**$^\bullet$	+0.10	−0.43	−1.30[c]	−	8.3×10^{-8}
$C_{12}H_{25}$-**3**$^+$	−	+0.11	−0.43	−1.31[c]	
$C_{12}H_{25}$-**3**$^\bullet$	+0.07	−0.47	−1.33[c]	−	1.0×10^{-7}
$C_{16}H_{33}$-**3**$^+$	−	+0.09	−0.45	−1.32[c]	
$C_{16}H_{33}$-**3**$^\bullet$	+0.07	−0.47	−1.35[c]	−	1.0×10^{-9}

[a] E/V vs SCE, 0.1 mol dm^{-3} Et_4NClO_4 in DMF, Pt electrode, scan rate 100 mV s^{-1}. [b] Measured on compaction pellets by a two-probe method at room temperature. [c] Irreversible or quasi-reversible waves. Values are calculated as $E^{red} = E^{pc}$(cathodic peak potential) + 0.03 V.

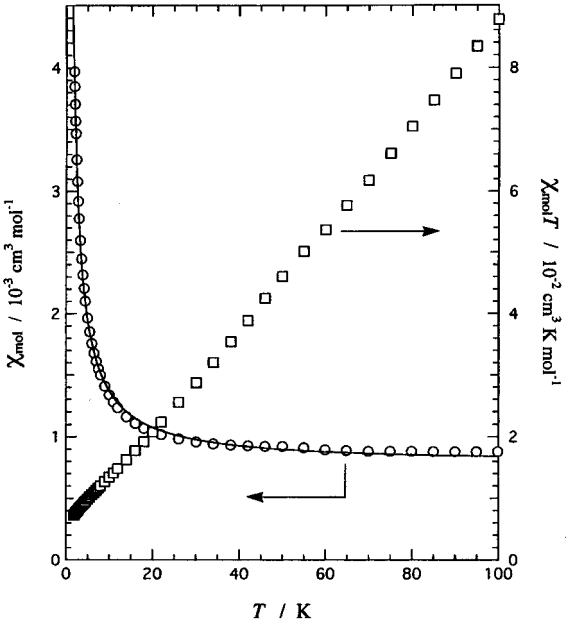

Figure 7. Temperature-dependence of magnetic susceptibility of CH_3-**3**$^\bullet$. The solid line represents the calculated χ_{mol} based on the modified Curie−Weiss equation (see text).

orders of magnitude (10^{-6} to 10^{-9} S cm^{-1}), indicating that the alkyl chain may affect the crystal packing. X-ray analysis of C_5H_{11}-**3**$^\bullet$ (Figure S4) revealed that the molecular geometry and two overlaps in the columnar stack closely resemble those in CH_3-**3**$^\bullet$ (Scheme 4 and Figures 4b, 5c, and 5d). The largest difference between the two packing patterns is that there is no short contact between columnar stacks in C_5H_{11}-**3**$^\bullet$, which may explain why its conductivity is less than that of CH_3-**3**$^\bullet$ by 2 orders of magnitude.

Finally, considering the recent interest in conducting magnetic multifunctional materials,[24] the magnetic properties of radical CH_3-**3**$^\bullet$ were also investigated by a SQUID magnetometer. Figure 7 shows the temperature-dependence of the molar magnetic susceptibility, which is obviously smaller than the value expected for a S =

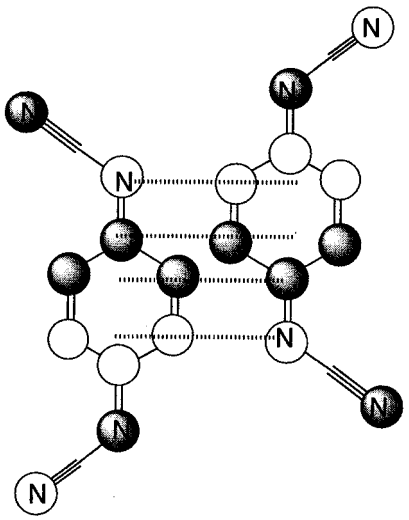

Figure 8. SOMO of DCNQI$^{-\bullet}$. Two molecules are shown to postulate the orbital interaction in the dyad of CH_3-**3**$^\bullet$ and C_5H_{11}-**3**$^\bullet$. The areas of the circles are arbitrary.

1/2 species. The data satisfactorily fit the Curie−Weiss equation with temperature-independent paramagnetism [$\chi_{mol} = C/(T - \theta) + N\alpha$], where C, θ, and $N\alpha$ are the Curie constant, Weiss temperature, and temperature-independent paramagnetic term, respectively. We obtained $C = 5.94 \times 10^{-3}$ cm^3 K mol^{-1}, $\theta = -0.018$ K, and $N\alpha = 7.79 \times 10^{-4}$ cm^3 mol^{-1}. The C value corresponds to a spin concentration of 1.6%, indicating the presence of strong antiferromagnetic coupling to make this specimen practically diamagnetic just like TCNQ$^{-\bullet}$ compounds.[25] The Curie spins are likely to arise from lattice defects. The negligible θ value can be rationalized in view of the low spin concentration.

The crystal structure of CH_3-**3**$^\bullet$ shown in Figure 5a suggests that antiferromagnetic coupling takes place within a dyad. The singly occupied molecular orbital (SOMO) of DCNNQI$^{-\bullet}$ is calculated based on the semiempirical MO theory and schematically shown in Figure 8. The "ring-over-double bond"-type dimerization gives rise to a considerably large SOMO−SOMO overlap because they are facing each other in-phase. The interdyad magnetic interaction is not yet clear, but the interplanar distance of 3.43 Å also suggests the presence of SOMO−SOMO overlap between dyads. The intra- and interdyad orbital overlaps seem responsible for the observed temperature-independent paramagnetism as well as semiconducting properties.

Conclusion

These results have shown that the novel radicals **2**$^\bullet$ and **3**$^\bullet$ can be isolated as crystalline stable solids, which prefer a zwitterionic structure (form B) rather than a neutral radical form (form A). Due to their high electrochemical amphotericity with E_{sum} ($\equiv E_1^{ox} - E_1^{red}$) of 0.48−0.54 V, they exhibit electrical conductivities of 10^{-5} to 10^{-9} S cm^{-1}, and thus represent a new motif for a single-component organic semiconductor. These values, however, are much lower than those of conventional multi-

(24) Sugano, T.; Fukasawa, T.; Kinoshita, M. *Synth. Met.* **1991**, *41−43*, 3281. Sugimoto, T.; Yamaga, S.; Kakai, M.; Ohmori, K.; Tsujii, M.; Nakatsuji, H.; Fujita, H.; Yamauchi, J. *Chem. Lett.* **1993**, 1361. Kumai, R.; Izuoka, A.; Sugawara, T. *Mol. Cryst. Liq. Cryst.* **1993**, *232*, 151. Fujiwara, H.; Kobayashi, H. *Chem. Commun.* **1999**, 2417.

(25) Fritchie, C. J., Jr.; Arthur, P., Jr. *Acta Crystallogr.* **1966**, *21*, 139. Reis, A. H., Jr.; Preston, L. D.; Williams, J. M.; Peterson, S. W.; Candela, G. A.; Swartzendruber, L. J.; Miller, J. S. *J. Am. Chem. Soc.* **1979**, *101*, 2756.

component conductors, perhaps due to the adoption of unfavorable packing arrangements such as a nonuniform columnar stack. Another factor that limits the present conductivities seems to be the predominant contribution of form B to the radicals. When the contributions of forms A and B are nearly equal, fractional charge-transfer would be achieved on the DCNNQI skeleton, which leads to a half-filled band structure to achieve higher conductivity. Studies involving exchange of the pyridinium unit for other quaternary heterocycles with much stronger electron affinity are now in progress.

Experimental Section

Preparation of Pyrazino-DCNNQI Derivatives (1a−f). To an ice-cooled yellow solution of $TiCl_4$ (0.30 mL, 2.74 mmol) in dry THF (23 mL) were added a solution of bis(trimethylsilyl)carbodiimide **6** (696 mg, 3.68 mmol) in 2 mL of dry THF and then a suspension of finely powdered quinone **1a**[11] (100 mg, 0.476 mmol) in 15 mL of dry THF under N_2. After the mixture was stirred for 80 min, it was poured into an ice-cooled buffer solution (1/30 mol dm^{-3} $Na_2HPO_4-KH_2PO_4$, 120 mL) and extracted with cold CH_2Cl_2. The combined extracts were washed with brine and dried over Na_2SO_4. Evaporation of solvent and recrystallization from CH_2Cl_2−hexane gave *N,N′*-dicyanopyrazino[2,3-*b*]naphthoquinodiimine **1a** (49 mg) as orange crystals in 40% yield. 2-(2-Pyridyl)-, 2-(3-pyridyl)-, and 2-(4-pyridyl)-substituted derivatives, **1c**−**e**, were also obtained by similar procedures in respective yields of 42%, 28%, and 40%.

To a solution of quinone **4b**[11] (103 mg, 0.284 mmol) in 10 mL of dry CH_2Cl_2 was added $TiCl_4$ (0.12 mL, 1.09 mmol) under N_2. To the resultant suspension of the complex was then added dropwise a solution of **6** (685 mg, 3.80 mmol) in 2 mL of dry CH_2Cl_2 over 10 min. After the entire mixture was stirred at room temperature for 4 h and then heated at reflux for 2.5 h, it was poured into water (100 mL) and extracted with CH_2Cl_2. The combined extracts were washed with brine and dried over Na_2SO_4. Evaporation of solvent and recrystallization from CH_2Cl_2−MeOH gave *N,N′*-dicyano-2,3-diphenylpyrazino[2,3-*b*]naphthoquinodiimine **1b** (84 mg) as orange crystals in 72% yield.

To a suspension of quinone **4f** (751 mg, 2.06 mmol) and CsF (3.70 g, 24.4 mmol) in dry THF (150 mL) was added dropwise a solution of **6** (3.34 g, 18.6 mmol) in 5 mL of dry THF over 10 min under N_2. After the mixture was stirred for 2 h at room temperature, it was poured into an ice-cooled buffer solution (1/30 mol dm^{-3} $Na_2HPO_4-KH_2PO_4$, 175 mL) and extracted with cold CH_2Cl_2. The combined extracts were washed with brine and dried over Na_2SO_4. Evaporation of solvent and recrystallization from CH_2Cl_2−hexane gave 2,3-bis(2-pyridyl)-*N,N′*-dicyanopyrazino[2,3-*b*]naphthoquinodiimine **1f** (674 mg) as orange needles in 79% yield. This material is the CH_2Cl_2-solvate and is efflorescent when exposed to air.

Data for **1a**: mp 252−270 °C (dec); ^{1}H NMR (200 MHz, $CDCl_3$) δ/ppm 9.24 (2H, s), 8.64−8.59 (2H, m), 7.95 (2H, AA′XX′); IR (KBr) 2140 cm^{-1}; EI-MS *m/z* 258 (M^+). Anal. Calcd for $C_{14}H_6N_6$: C, 65.11; H, 2.34; N, 32.54. Found: C, 64.63; H, 2.58; N, 32.04. Data for **1b**: mp 280−287 °C (dec); ^{1}H NMR (90 MHz, $CDCl_3$) δ/ppm 8.57 (2H, AA′XX′), 7.90 (2H, AA′XX′), 7.80−7.60 (4H, m), 7.50−7.30 (6H, m); IR (KBr) 2143 cm^{-1}; UV−vis (DMF) λ_{max} 438 (sh, log ϵ 3.69), 368 (4.46), 358 (4.46), 314 (4.38), 306 (sh, 4.37) nm; EI-MS *m/z* (relative intensity) 410 (M^+, 100), 409 (29). Anal. Calcd for $C_{26}H_{14}N_6$: C, 76.09; H, 3.44; N, 20.48. Found: C, 75.62; H, 3.55; N, 20.32. Data for **1c**: orange powder (1,2-dichloroethane−hexane), mp 235−255 °C (dec); ^{1}H NMR (200 MHz, $CDCl_3$) δ/ppm 10.34 (1H, s), 9.06 (1H, ddd, J = 7.9, 1.1, 1.0 Hz), 8.65 (1H, ddd, J = 4.8, 1.8, 1.0 Hz), 8.65−8.60 (2H, m), 8.03 (1H, ddd, J = 7.9, 7.7, 1.8 Hz), 7.97−7.92 (2H, m), 7.52 (1H, ddd, J = 7.7, 4.8, 1.1 Hz); IR (KBr) 2137 cm^{-1}; EI-MS *m/z* 335 (M^+). Anal. Calcd for $C_{19}H_9N_7 \cdot 0.75H_2O$: C, 65.42; H, 3.03; N, 28.11. Found: C, 65.73; H, 2.98; N, 27.76. Data for **1d**: orange powder (CH_2Cl_2−hexane), mp 209.5−211 °C (dec); ^{1}H NMR (200 MHz, $CDCl_3$) δ/ppm 9.76 (1H, s), 9.57 (1H, dd, J = 2.1, 0.8 Hz), 9.08 (1H, ddd, J = 8.1, 2.1, 1.8 Hz), 8.87 (1H, dd, J = 5.0, 1.8 Hz) 8.65−8.50 (2H, m), 7.98−7.93 (2H, m), 7.65 (1H, ddd, J = 8.1, 5.0, 0.8 Hz); IR (KBr) 2138 cm^{-1}; EI-MS *m/z* 335 (M^+). Anal. Calcd for $C_{19}H_9N_7 \cdot H_2O$: C, 64.59; H, 3.14; N, 27.75. Found: C, 64.83; H, 3.12; N, 27.85. Data for **1e**: orange powder (CH_2Cl_2−hexane), mp 203−226 °C (dec); ^{1}H NMR (200 MHz, $CDCl_3$) δ/ppm 9.75 (1H, s), 8.97 (2H, AA′BB′), 8.66−8.61 (2H, m), 8.38 (2H, AA′BB′), 7.99−7.94 (2H, m); IR (KBr) 2138 cm^{-1}; EI-MS *m/z* (relative intensity) 335 (M^+, 63), 334 (100). Anal. Calcd for $C_{19}H_9N_7 \cdot 0.5H_2O$: C, 66.27; H, 2.93; N, 28.47. Found: C, 65.82; H, 2.90; N, 28.56. Data for **1f**: mp 254−268 °C (dec); ^{1}H NMR (200 MHz, $CDCl_3$) δ/ppm 8.75 (2H, ddd, J = 7.8, 1.0, 0.8 Hz), 8.62 (2H, AA′XX′), 8.31 (2H, ddd, J = 4.9, 1.7, 0.8 Hz), 8.01 (2H, ddd, J = 7.8, 7.7, 1.7 Hz), 7.94 (2H, AA′XX′), 7.33 (2H, ddd, J = 7.7, 4.9, 1.0 Hz); IR (KBr) 2143 cm^{-1}; UV−vis (DMF) λ_{max} 352 (log ϵ 4.47), 314 (4.45) nm, EI-MS *m/z* 412 (M^+). Anal. Calcd for $C_{24}H_{12}N_8 \cdot 0.5CH_2Cl_2$: C, 64.69; H, 2.88; N, 24.63. Found: C, 64.34; H, 3.04; N, 24.50.

Preparation of Anion Radical Salt of 1b. A dry CH_2Cl_2 solution of **1b** (18 mg, 0.043 mmol) containing Et_4NClO_4 (0.05 mol dm^{-3}) was electrochemically reduced by a constant current of 15 μA in an H-tube. Pt wires were used as the working and counter electrodes. Anion radical salt [Et_4N^+(**1b**)$_2^{-\bullet}$] was deposited as black needles, which were collected by suction (12 mg, yield 60%): mp 207−221 °C (dec), IR (KBr) 2096 cm^{-1}; UV−vis (DMF) λ_{max} 588 (log ϵ 4.32), 534 (4.14), 450 (sh, 4.01), 374 (sh, 4.60), 340 (4.77), 322 (sh, 4.68), 298 (sh, 4.61). Anal. Calcd for $C_{60}H_{48}N_{13} \cdot 2H_2O$: C, 73.00; H, 5.31; N, 18.45. Found: C, 73.45; H, 5.24; N, 18.23.

Preparation of Quaternary Salts (2d$^+$TfO$^-$, 2e$^+$TfO$^-$, and C_nH_{2n+1}-3$^+$TfO$^-$). To a solution of **1d** (26 mg, 0.0769 mmol) in dry CH_2Cl_2 (30 mL) was added CH_3OTf (0.050 mL, 0.44 mmol) under N_2. After the mixture was stirred for 14 h, filtration of the deposited precipitates gave 3-(*N,N′*-dicyanopyrazino[2,3-b]naphthoquinodiimin-2-yl)-1-methylpyridinium triflate **2d**$^+$TfO$^-$ (27 mg) as a yellow powder in 71% yield. Similarly, **2e**$^+$TfO$^-$ and CH_3-**3**$^+$TfO$^-$ were obtained from **1e** and **1f** in respective yields of 91% and 82%. By using *n*-C_nH_{2n+1}OTf[26] (n = 3, 5, 8, 12, and 16) in place of CH_3OTf, C_nH_{2n+1}-**3**$^+$TfO$^-$ salts were obtained from **1f** in respective yields of 82%, 79%, 50%, 40%, and 40%. In cases of cations with a long alkyl chain (n = 12 and 16), the addition of ether and hexane was necessary to deposit the quaternary salts before filtration.

Data for **2d**$^+$TfO$^-$: mp 139−161 °C (dec); ^{1}H NMR (200 MHz, CD_3CN) δ/ppm 9.97 (1H, br. s), 9.83 (1H, s), 9.44 (1H, d, J = 8.2 Hz), 8.81 (1H, d, J = 6.2 Hz) 8.62−8.57 (2H, m), 8.72 (1H, dd, J = 8.2, 6.2 Hz), 8.04−8.00 (2H, m), 4.47 (3H, s); IR (KBr) 2149, 1275, 1256 cm^{-1}; FAB-MS (relative intensity) *m/z* 351 (71), 350 (M^+, 100). Anal. Calcd for $C_{20}H_{12}N_7 \cdot CF_3SO_3 \cdot H_2O$: C, 48.74; H, 2.73; N, 18.95; S, 6.20. Found: C, 48.84; H, 2.77; N, 18.89; S, 6.21. Data for **2e**$^+$TfO$^-$: yellow powder, mp 227.5−246 °C (dec); ^{1}H NMR (200 MHz, CD_3CN) δ/ppm 9.93 (1H, s), 9.06 (2H, AA′BB′), 8.90 (2H, AA′BB′), 8.62−8.57 (2H, m), 8.04−8.00 (2H, m), 4.49 (3H, s); IR (KBr) 2144, 1160 cm^{-1}; FAB-MS (relative intensity) *m/z* 351 (64), 350 (M^+, 100). Anal. Calcd for $C_{20}H_{12}N_7 \cdot CF_3SO_3 \cdot 0.5H_2O$: C, 49.61; H, 2.58; N, 19.28; S, 6.31. Found: C, 49.50; H, 2.50; N, 19.06 S, 6.47. Data for CH_3-**3**$^+$TfO$^-$: yellow powder, mp 252−260 °C (dec); ^{1}H NMR (200 MHz, acetone-d_6) δ/ppm 9.48 (1H, dd, J = 6.4, 1.2 Hz), 9.13 (1H, ddd, J = 7.8, 1.2, 1.0 Hz), 8.82 (1H, ddd, J = 8.1, 7.3, 1.2 Hz), 8.68 (2H, m), 8.46 (1H, ddd, J = 7.3, 6.4, 1.2 Hz), 8.37 (1H, ddd, J = 4.6, 1.6, 1.0 Hz), 8.26 (1H, dd, J = 8.1, 1.2 Hz), 8.19 (2H, ddd, J = 7.8, 7.6, 1.6 Hz), 8.15 (2H, m), 7.59 (1H, ddd, J = 7.6, 4.6, 1.2 Hz), 5.63 (2H, s, CH_2Cl_2), 4.65 (3H, s); IR (KBr) 2152, 1258 cm^{-1}; UV−vis (DMF) λ_{max} 324 (log ϵ 4.45), 284 (4.38) nm; FAB-MS *m/z* 427 (M^+). Anal. Calcd for $C_{25}H_{15}N_8 \cdot CF_3SO_3 \cdot H_2O \cdot CH_2Cl_2$: C, 47.73; H, 2.82; N, 16.49. Found: C, 48.08; H, 2.63; N, 16.69. Data for C_3H_7-**3**$^+$TfO$^-$: yellow powder, mp 220.5−226 °C (dec); ^{1}H NMR (200 MHz,

(26) Beard, C. D.; Baum, K.; Grakauskas, V, *J. Org. Chem.* **1973**, *38*, 3673.

CD_3CN) δ/ppm 9.07 (1H, ddd, J = 7.9, 1.0, 1.0 Hz), 8.96 (1H, dd, J = 6.2, 1.4 Hz), 8.61 (2H, m), 8.53 (1H, ddd, J = 8.1, 7.8, 1.4 Hz), 8.24 (1H, ddd, J = 4.7, 1.7, 1.0 Hz), 8.17 (1H, ddd, J = 7.8, 6.2, 1.5 Hz), 8.09 (1H, ddd, J = 7.9, 7.7, 1.7 Hz), 8.06 (2H, m), 7.86 (1H, dd, J = 8.1, 1.5 Hz), 7.47 (1H, ddd, J = 7.7, 4.7, 1.0 Hz), 4.71 (1H, ddd, J = 14.0, 8.6, 6.6 Hz), 4.39 (1H, ddd, J = 14.0, 9.0, 6.6 Hz), 1.96−1.91 (2H, m), 0.85 (3H, t, J = 7.4 Hz); IR (KBr) 2148, 1260 cm^{-1}; FAB-MS m/z 455 (M^+). Anal. Calcd for $C_{27}H_{19}N_8{\cdot}CF_3SO_3{\cdot}H_2O$: C, 54.02; H, 3.40; N, 18.00. Found: C, 53.63; H, 3.31; N, 17.66. Data for C_5H_{11}-**3**$^+$-TfO^-: pale yellow powder, mp 256−267 °C (dec); ^{1}H NMR (200 MHz, CD_3CN) δ/ppm 9.07 (1H, ddd, J = 7.9, 1.0, 1.0 Hz), 8.95 (1H, dd, J = 6.3, 1.3 Hz), 8.64−8.59 (2H, m), 8.52 (1H, ddd, J = 8.1, 7.8, 1.3 Hz), 8.24 (1H, ddd, J = 4.8, 1.8, 1.0 Hz), 8.17 (1H, ddd, J = 7.8, 6.3, 1.4 Hz), 8.09 (1H, ddd, J = 7.9, 7.7, 1.8 Hz), 8.04−8.02 (2H, m), 7.85 (1H, dd, J = 8.1, 1.4 Hz), 7.47 (1H, ddd, J = 7.7, 4.8, 1.0 Hz), 4.84 (1H, ddd, J = 13.6, 9.2, 6.4 Hz), 4.52 (1H, ddd, J = 13.6, 8.9, 6.2 Hz), 1.96−1.91 (2H, m), 1.22−1.17 (4H, m), 0.80−0.73 (3H, m); IR (KBr) 2157, 1273 cm^{-1}; FAB-MS m/z 483 (M^+). Anal. Calcd for $C_{29}H_{23}N_8{\cdot}CF_3SO_3{\cdot}1.5H_2O$: C, 54.62; H, 3.97; N, 16.99. Found: C, 54.74; H, 3.66; N, 16.82. Data for C_8H_{17}-**3**$^+TfO^-$: pale yellow powder, mp 240.5−250 °C (dec); ^{1}H NMR (200 MHz, CD_3CN) δ/ppm 9.07 (1H, ddd, J = 7.8, 1.0, 0.8 Hz), 8.94 (1H, dd, J = 6.1, 1.0 Hz), 8.67−8.57 (2H, m), 8.52 (1H, ddd, J = 8.0, 7.9, 1.0 Hz), 8.23 (1H, ddd, J = 4.7, 1.7, 0.8 Hz), 8.17 (1H, ddd, J = 7.9, 6.1, 1.5 Hz), 8.09 (2H, ddd, J = 7.8, 7.7, 1.7 Hz), 8.07−8.03 (2H, m), 7.86 (1H, dd, J = 8.0, 1.5 Hz), 7.48 (1H, ddd, J = 7.7, 4.7, 1.0 Hz), 4.71 (1H, ddd, J = 13.8, 9.0, 6.2 Hz), 4.38 (1H, ddd, J = 13.8, 9.0, 6.4 Hz), 1.96−1.91 (2H, m), 1.01 (10H, m), 0.76 (3H, t, J = 5.5 Hz); IR (KBr) 2144, 1261 cm^{-1}; FAB-MS m/z 525 (M^+). Anal. Calcd for $C_{32}H_{29}N_8{\cdot}CF_3SO_3{\cdot}0.5H_2O$: C, 57.97; H, 4.42; N, 16.39. Found: C, 57.70; H, 4.45; N, 16.10. Data for $C_{12}H_{25}$-**3**$^+TfO^-$: yellow powder, mp 95−124 °C (dec); ^{1}H NMR (200 MHz, CD_3CN) δ/ppm 9.07 (1H, ddd, J = 7.9, 1.1, 0.9 Hz), 8.94 (1H, dd, J = 6.3, 1.2 Hz), 8.67−8.58 (2H, m), 8.52 (1H, ddd, J = 8.0, 7.9, 1.2 Hz), 8.23 (1H, ddd, J = 4.6, 1.8, 0.9 Hz), 8.17 (1H, ddd, J = 7.9, 6.3, 1.4 Hz), 8.09 (1H, ddd, J = 7.9, 7.7, 1.8 Hz), 8.10−8.02 (2H, m), 7.86 (1H, dd, J = 8.0, 1.4 Hz), 7.47 (1H, ddd, J = 7.7, 4.6, 1.1 Hz), 4.71 (1H, ddd, J = 13.8, 8.8, 6.2 Hz), 4.38 (1H, ddd, J = 13.8, 9.0, 6.2 Hz), 1.96−1.91 (2H, m), 1.16 (18H, m), 0.85 (3H, t, J = 6.6 Hz); IR (KBr) 2922, 2150, 1259 cm^{-1}; FAB-MS m/z 581 (M^+). Anal. Calcd for $C_{36}H_{37}N_8{\cdot}CF_3SO_3{\cdot}0.5H_2O$: C, 60.07; H, 5.18; N, 15.15; S, 4.33. Found: C, 60.36; H, 5.17; N, 14.78; S, 4.64. Data for $C_{16}H_{33}$-**3**$^+TfO^-$: yellow powder, mp 87−121 °C (dec); ^{1}H NMR (200 MHz, CD_3CN) δ/ppm 9.07 (1H, ddd, J = 8.0, 1.1, 1.0 Hz), 8.94 (1H, dd, J = 6.3, 1.3 Hz), 8.66−8.58 (2H, m), 8.52 (1H, ddd, J = 8.0, 7.8, 1.3 Hz), 8.23 (1H, ddd, J = 5.0, 1.8, 1.1 Hz), 8.17 (1H, ddd, J = 7.8, 6.3, 1.4 Hz), 8.08 (1H, ddd, J = 8.0, 7.7, 1.8 Hz), 8.04 (2H, m), 7.86 (1H, dd, J = 8.0, 1.4 Hz), 7.47 (1H, ddd, J = 7.5, 5.0, 1.0 Hz), 4.71 (1H, ddd, J = 13.8, 9.0, 6.0 Hz), 4.38 (1H, ddd, J = 13.8, 8.8, 6.2 Hz), 1.96−1.91 (2H, m), 1.30−1.11 (26H, m), 0.87 (3H, t, J = 6.4 Hz); IR (KBr) 2917, 2150, 1268 cm^{-1}; FAB-MS m/z 637 (M^+). Anal. Calcd for $C_{40}H_{45}N_8{\cdot}CF_3SO_3{\cdot}0.5H_2O$: C, 61.87; H, 5.83; N, 14.08. Found: C, 62.14; H, 5.69; N, 14.06.

Preparation of Stable Radicals (2d$^\bullet$, 2e$^\bullet$, and C_nH_{2n+1}-3$^\bullet$). A dry MeCN solution of **2d**$^+TfO^-$ (10 mg, 0.020 mmol) containing Et_4NTfO (0.05 mol dm^{-3}) was electrochemically reduced by a constant current of 15 μA in an H-tube. Pt wires were used as the working and counter electrodes. 3-(*N*,*N*′-Dicyanopyrazino[2,3-*b*]naphthoquinodiimin-2-yl)-1-methylpyridyl **2d**$^\bullet$ was gradually deposited as black-violet crystals, which were collected by suction (6 mg, yield 77%). Similarly, **2e**$^\bullet$ and C_nH_{2n+1}-**3**$^\bullet$ (n = 1, 3, 5, 8, 12, and 16) were obtained from **2e**$^+TfO^-$ and C_nH_{2n+1}-**3**$^+TfO^-$ in respective yields of 88%, 72%, 71%, 87%, 46%, 68%, and 63%.

Data for **2d**$^\bullet$: mp 243−251 °C (dec); IR (KBr) 2092 cm^{-1}; FAB-MS (relative intensity) m/z 352 (100), 351 (36), 350 (M^+, 16). Anal. Calcd for $C_{20}H_{12}N_7{\cdot}1.5H_2O$: C, 63.65; H, 4.01; N, 25.97. Found: C, 63.78; H, 3.91; N, 25.46. Data for **2e**$^\bullet$: black-violet crystals, mp 260−273 °C (dec); IR (KBr) 2091 cm^{-1}; FAB-MS (relative intensity) m/z 352 (100), 351 (50), 350 (M^+, 18). Anal. Calcd for $C_{20}H_{12}N_7{\cdot}2H_2O$: C, 62.16; H, 4.17; N, 25.37. Found: C, 62.21; H, 3.86; N, 25.49. Data for CH_3-**3**$^\bullet$: black crystals, mp 190−198 °C (dec); IR (KBr) 2107 cm^{-1}; UV−vis (DMF) λ_{max} 596 (log ϵ 4.09), 550 (3.94), 460 (3.76), 336 (4.86), 326 (sh, 4.85), 284 (4.74) nm. Anal. Calcd for $C_{25}H_{15}N_8{\cdot}H_2O$: C, 67.41; H, 3.85; N, 25.15. Found: C, 67.09; H, 3.67; N, 24.74. Data for C_3H_7-**3**$^\bullet$: black crystals, mp 70−78 °C (dec); IR (KBr) 2107 cm^{-1}. Anal. Calcd for $C_{27}H_{19}N_8{\cdot}1.5H_2O$: C, 67.21; H, 4.60; N, 23.22. Found: C, 66.85; H, 4.60; N, 23.18. Data for C_5H_{11}-**3**$^\bullet$: black-violet crystals, mp 218−225 °C (dec); IR (KBr) 2107 cm^{-1}; UV−vis (DMF) λ_{max} 596 (log ϵ 4.17), 550 (4.03), 456 (3.82), 338 (4.48), 326 (sh, 4.45), 286 (4.29) nm. Anal. Calcd for $C_{29}H_{23}N_8{\cdot}2H_2O$: C, 67.04; H, 5.24; N, 21.57. Found: C, 66.50; H, 5.09; N, 21.32. Data for C_8H_{17}-**3**$^\bullet$: black-violet crystals, mp 100−108 °C (dec); IR (KBr) 2097 cm^{-1}; UV−vis (DMF) λ_{max} 598 (log ϵ 4.26), 550 (4.11), 460 (3.90), 338 (4.56), 326 (sh, 4.53), 286 (4.36) nm. Anal. Calcd for $C_{32}H_{29}N_8{\cdot}0.75H_2O$: C, 71.29; H, 5.70; N, 20.78. Found: C, 71.44; H, 5.70; N, 20.71. Data for $C_{12}H_{25}$-**3**$^\bullet$: black-violet crystals, mp 93−106 °C (dec); IR (KBr) 2100 cm^{-1}. Anal. Calcd for $C_{36}H_{37}N_8{\cdot}0.5H_2O$: C, 73.19; H, 6.48; N, 18.97. Found: C, 73.44; H, 6.40; N, 18.82. Data for $C_{16}H_{33}$-**3**$^\bullet$: black-violet crystals, mp 193−207 °C (dec); IR (KBr) 2101 cm^{-1}. Anal. Calcd for $C_{40}H_{45}N_8{\cdot}0.5H_2O$: C, 74.27; H, 7.17; N, 17.32. Found: C, 73.92; H, 7.24; N, 17.11.

Preparation of Quinones (4c−f). To a solution of 2,3-diaminonaphthoquinone[12] (2.00 g, 10.6 mmol) in dry DMSO (25 mL) was added 2-(bromoacetyl)pyridinium bromide[27] (3.59 g, 12.8 mmol). After the mixture was stirred at room temperature for 3 h, it was poured into water (250 mL) and extracted with CH_2Cl_2. The combined extracts were washed with water and dried over Na_2SO_4. Evaporation of solvent and chromatographic separation on Al_2O_3 (CH_2Cl_2) gave 2-(2-pyridyl)-pyrazino[2,3-*b*]naphthoquinone **4c** (913 mg) as pale yellow needles in 30% yield. 2-(3-Pyridyl) and 2-(4-pyridyl) derivatives, **4d** and **4e**, were obtained by similar condensation reactions of **6** with 3- and 4-(bromoacetyl)pyridinium bromide, respectively, in yields of 37% and 30%. In the latter two cases, crude products were purified by sublimation (0.01 Torr; 240−260 °C for **4d** and 260−270 °C for **4e**).

To a solution of 2,3-diaminonaphthoquinone (2.46 g, 13.1 mmol) in EtOH (170 mL) was added 2,2′-pyridil (3.15 g, 14.4 mmol), and the mixture was heated at reflux for 15 h. A tan powder precipitated on cooling, which was collected by suction. Recrystallization from CH_2Cl_2−EtOH gave 2,3-bis(2-pyridyl)-pyrazino[2,3-*b*]naphthoquinone **4f** (3.04 g) as pale yellow needles in 64% yield.

Data for **4c**: mp 265−266 °C; ^{1}H NMR (200 MHz, $CDCl_3$) δ/ppm 9.55 (1H, s), 9.47 (1H, dd, J = 2.6, 0.6 Hz), 8.85 (1H, dd, J = 4.8, 1.7 Hz), 8.65 (1H, ddd, J = 8.0, 2.0, 1.7 Hz), 8.47 (2H, m), 7.94 (2H, m), 7.57 (1H, ddd, J = 8.0, 4.8, 0.6 Hz); IR (KBr) 1686, 1677 cm^{-1}; EI-MS m/z 287 (M^+). Anal. Calcd for $C_{17}H_9N_3O_2{\cdot}0.25H_2O$: C, 69.98; H, 3.28; N, 14.40. Found: C, 70.28; H, 3.42; N, 14.36. Data for **4d**: yellow needles, mp 269−271.5 °C; ^{1}H NMR (200 MHz, $CDCl_3$) δ/ppm 9.55 (1H, s), 9.47 (1H, dd, J = 2.0, 0.6 Hz), 8.85 (1H, dd, J = 4.8, 1.7 Hz), 8.65 (1H, ddd, J = 8.0, 2.0, 1.7 Hz) 8.47 (2H, m), 7.94 (2H, m), 7.57 (1H, ddd, J = 8.0, 4.8, 0.6 Hz); IR (KBr) 1686, 1677 cm^{-1}; EI-MS m/z 287 (M^+). Anal. Calcd for $C_{17}H_9N_3O_2{\cdot}0.5H_2O$: C, 68.92; H, 3.40; N, 14.18. Found: C, 68.59; H, 3.39; N, 13.98 Data for **4e**: yellow needles, mp 299−300 °C ^{1}H NMR (200 MHz, $CDCl_3$) δ/ppm 9.57 (1H, s), 8.91 (2H, AA′BB′), 8.48 (2H, m), 8.18 (2H, AA′BB′), 7.95 (2H, m); IR (KBr) 1682 cm^{-1}; EI-MS m/z 287 (M^+). Anal. Calcd for $C_{17}H_9N_3O_2{\cdot}0.25H_2O$: C, 69.97; H, 3.28; N, 14.40. Found: C, 70.14; H, 3.39; N, 14.49. Data for **4f**: mp 289−292 °; ^{1}H NMR (200 MHz, $CDCl_3$) δ/ppm 8.47 (2H, AA′XX′), 8.31 (2H, ddd, J = 4.8, 1.2, 1.2 Hz), 8.26 (2H, ddd, J = 7.8, 1.2, 1.2 Hz), 7.98−7.85 (4H, m), 7.29 (2H, ddd, J = 7.8, 4.8, 1.2 Hz); IR (KBr) 1694, 1672 cm^{-1}; EI-MS m/z 364 (M^+). Anal. Calcd for $C_{22}H_{12}N_4O_2$: C, 72.52; H, 3.32; N, 15.38. Found: C, 72.24; H, 3.77; N, 15.40.

Preparation of Pyrazino-TCNNQ Derivatives (7f). To a solution of quinone **4f** (500 mg, 1.37 mmol) in 40 mL of dry

(27) Wingfield, H. N., Jr. *J. Org. Chem.* **1959**, *24*, 872.

CH_2Cl_2 was added $TiCl_4$ (0.60 mL, 5.47 mmol) under N_2. To the resultant suspension of the complex was then added dropwise a solution of malononitrile (458 mg, 4.93 mmol) and dry pyridine (4.5 mL, 55.6 mmol) in 20 mL of dry CH_2Cl_2 over 1 h at −20 °C. After the entire mixture was stirred at this temperature for 3 h, it was poured into water (200 mL) and extracted with CH_2Cl_2. The combined extracts were washed with brine and dried over Na_2SO_4. Evaporation of solvent and chromatographic separation on SiO_2 (AcOEt/CH_2Cl_2, 1:30) gave 2,3-bis(2-pyridyl)-11,11,12,12-tetracyanopyrazino[2,3-*b*]naphthoquinodimethane **7f** (343 mg) as a pale yellow powder in 54% yield: mp 246−258 °C (dec); ^{1}H NMR (200 MHz, $CDCl_3$) δ/ppm 8.58 (2H, AA′XX′), 8.36 (2H, ddd, J = 8.1, 1.1, 1.1 Hz),8.31 (2H, ddd, J = 4.9, 2.0, 1.1 Hz), 7.94 (2H, ddd, J = 8.1, 8.1, 2.0 Hz), 7.87 (2H, AA′XX′), 7.31 (2H, ddd, J = 8.1, 4.9, 1.1 Hz); IR (KBr) 2215 cm^{-1}; UV−vis (MeCN) λ_{max} 366 (log ϵ 4.56), 312 (4.45), 226 (4.52) nm, EI-MS m/z 460 (M^+). Anal. Calcd for $C_{28}H_{12}N_8$·0.75CH_2Cl_2: C, 65.88; H, 2.60; N, 21.38. Found: C, 65.76; H, 2.79; N, 22.24.

Measurement of Redox Potentials. Oxidation potentials (E^{ox}) were measured by cyclic voltammetry in dry MeCN or dry DMF containing 0.1 mol dm^{-3} Et_4NClO_4 as a supporting electrolyte. Ferrocene undergoes 1e-oxidation at +0.38 V in MeCN or at +0.44 V in DMF under similar conditions. All of the values shown in the text are in E/V vs SCE, and Pt was used as the working electrode. In the case of irreversible waves, half-wave potentials were estimated from the cathodic peak potentials (E^{pc}) as $E^{red} = E^{pc}$+ 0.03 V.

X-ray Analyses. Crystal data for **1f**·CH_2Cl_2: $C_{25}H_{14}N_8Cl_2$, M 497.35, efflorescent orange needles by recrystallization from CH_2Cl_2, 0. 7 × 0.1 × 0.05 mm, triclinic P1bar, a = 11.444(1), b = 16.371(3), c = 6.1366(6) Å, α= 96.219(2), β = 102.977(2), γ = 78.624(4)°, V = 1095.9(2) Å^3, ρ (Z = 2) = 1.507 g cm^{-1}. A total of 4453 unique data points ($2\theta_{max}$ = 55.6°) were measured at T = 120 K on a Rigaku Mercury CCD camera apparatus (Mo−Kα radiation, λ= 0.71069 Å). Numerical absorption correction was applied (μ = 3.30 cm^{-1}). The structure was solved by the direct method and refined by the full-matrix least-squares method on F with anisotropic temperature factors for non-hydrogen atoms. Hydrogen atoms were picked up from the D-map. The final R and Rw values are 0.043 and 0.057 for 3374 reflections with $I > 3\sigma I$ and 315 parameters. The maximum residual electron density is 0.35 e Å^{-3}.

Crystal data for **7f**: $C_{28}H_{12}N_8$, M 460.46, yellow plates from $CHCl_3$, 0.3 × 0.15 × 0.1 mm, triclinic P1bar, a = 10.694(8), b = 13.104(7), c = 8.102(5) Å, α = 97.82(5), β = 101.07(6), γ = 76.35(5)°, V = 1077.8(12) Å^3, ρ (Z = 2) = 1.419 g cm^{-1}. A total of 3829 unique data points ($2\theta_{max}$ = 50°) were measured at T = 286 K by a Rigaku AFC-5R four-circle diffractometer with an $\omega-2\theta$ scan mode (Mo−Kα radiation, λ = 0.71069 Å). No absorption correction was applied (μ = 0841 cm^{-1}). The structure was solved by the direct method and refined by the block-diagonal least-squares method on F with anisotropic temperature factors for non-hydrogen atoms. Hydrogen atoms were picked up from the D-map and included in the refinement with isotropic temperature factors. The final R value is 0.090 for 2054 reflections with $F > 3\sigma F$ and 374 parameters. The maximum residual electron density is 0.40 e Å^{-3}.

Crystal data for CH_3-**3**$^{\bullet}$: $C_{25}H_{15}N_8$, M 427.45, black plates by electrocrystallization from MeCN containing 0.05 M $Et_4N^+TfO^-$, 0.25 × 0.1 × 0.1 mm, monoclinic $P2_1/c$, a = 8.089-(3), b = 11.916(2), c = 20.983(3) Å, β = 97.96(3), V = 2003.0-(8) Å^3, ρ (Z = 4) = 1.417 g cm^{-1}. A total of 2983 unique data points ($2\theta_{max}$ = 120°) were measured at T = 286 K with an $\omega-2\theta$ scan mode (Cu−Kα radiation, λ = 1.5418 Å). Absorption correction was applied by means of the empirical Ψ-scan method (μ = 6.87 cm^{-1}). The structure was solved by the direct method and refined by the block-diagonal least-squares method on F with anisotropic temperature factors for non-hydrogen atoms. Hydrogen atoms were located at the calculated positions and included in the refinement with isotropic temperature factors. The final R value is 0.079 for 1677 reflections with $F > 3\sigma F$ and 359 parameters. The maximum residual electron density is 0.38 e Å^{-3}.

Crystal data for n-C_5H_{11}-**3**$^{\bullet}$·2H_2O: $C_{29}H_{27}N_8O_2$, M 519.59, black needles by electrocrystallization from MeCN containing 0.05 M $Et_4N^+TfO^-$, 0.25 × 0.05 × 0.05 mm, triclinic P1bar, a = 11.987(2), b = 13.980(1), c = 7.679(1) Å, α= 92.30(1), β = 91.09(1), γ = 99.03(1)°, V = 1284.8(2) Å^3, ρ (Z = 2) = 1.343 g cm^{-1}. A total of 3529 unique data points ($2\theta_{max}$ = 115°) were measured at T = 286 K with $\omega-2\theta$ scan mode (Cu−Kα radiation, λ = 1.5418 Å). Absorption correction was applied by means of the empirical Ψ-scan method (μ = 6.81 cm^{-1}). The structure was solved by the direct method and refined by the block-diagonal least-squares method on F with anisotropic temperature factors for non-hydrogen atoms. Hydrogen atoms were located at the calculated positions and included in the refinement with isotropic temperature factors. The final R value is 0.076 for 2183 reflections with $F > 3\sigma F$ and 445 parameters. The maximum residual electron density is 0.36 e Å^{-3}.

Measurement of Electrical Conductivity of Radicals. Powder conductivities were measured on compaction samples by a two-probe method at room temperature. The temperature-dependence measurement was conducted on a specimen of CH_3-**3**$^{\bullet}$ (0.1 × 0.05 × 0.075 mm) by a two-probe method with a cooling rate of 2 K min^{-1} to 170 K. Anisotropy of the conductivity could not be measured since only tiny needlelike crystals were obtained. The values of σ and E_a for single-crystalline CH_3-**3**$^{\bullet}$ are those along the needle axis.

Measurement of Magnetic Properties of Radical CH_3-3$^{\bullet}$. Magnetic susceptibility was measured on a Quantum Design MPMS SQUID magnetometer. A sample cell was filled with a polycrystalline sample of CH_3-**3**$^{\bullet}$ (19.51 mg). The measurement was taken over the temperature range of 1.8 to 100 K at 0.5000 T. Background data of the cell were separately measured under the same conditions, and the diamagnetic contribution of the sample itself was estimated from Pascal's constants.

Acknowledgment. This work was supported by the Ministry of Education, Science and Culture, Japan (Grant Nos. 10146101 and 06243105). Financial support from the Casio Science Promotion Foundation and a Research Grant from the Iwatani Naoji Foundation (to T.S.) is gratefully acknowledged.

Supporting Information Available: Ortep drawings (Figures S1−S4) and structural data for the X-ray analyses (positional and thermal parameters; bond distances and angles) of **1f**·CH_2Cl_2, CH_3-**3**$^{\bullet}$, C_5H_{11}-**3**$^{\bullet}$·2H_2O, and **7f**. This material is available free of charge via the Internet at http://pubs.acs.org.

JO001352R